Low-pressure fabrication of IR-transparent Y_2O_3 via spark plasma sintering

Elnaz Irom ✉, *Mohammad Zakeri, Ali Sedaghat Ahangari Hossein Zadeh, Saman Safian, Ali Rahbari*

Ceramic Department, Materials and Energy Research Center (MERC), Tehran, P.O. Box 14155-4777, Iran
✉ *E-mail: e.irom@merc.ac.ir*

Published in Micro & Nano Letters; Received on 24th April 2016; Accepted on 4th July 2016

Different pressures of 80 and 90 MPa were applied to produce Y_2O_3 ceramics by spark plasma sintering in this work. Effects of pressure were investigated on densification, microstructure, infrared (IR) transmission and mechanical properties. It was found that applying higher pressure led to finer microstructure and consequently higher hardness and fracture toughness. An IR-transparent Y_2O_3 ceramic with 60% transmission at wavelength of 5 μm was obtained by sintering at 1300°C under uniaxial pressure of 90 MPa. This sample had an average grain size of 0.76 μm and hardness and fracture toughness of 9.37 GPa and 1.60 MPa.$m^{1/2}$, respectively.

1. Introduction: Y_2O_3 oxide ceramic is a desirable infrared (IR) material which is widely used in IR technology. It is a high-temperature, corrosion-resistant ceramic with a melting point of 2430°C and has satisfying optical and thermal properties for Mid-IR windows and domes application. It is also used as solid state laser gain media and scintillation detectors [1–3].

Single crystalline Y_2O_3 fabrication is quite troublesome due to its high melting point [4]. In recent decades, Y_2O_3 optical bodies have been produced by different methods such as pressureless sintering, and procedures which apply pressure and sintering simultaneously like hot pressing and hot isostatic pressing [2, 5, 6]. These procedures mostly result in coarse microstructure which is not valuable for IR technology application due to low mechanical properties. Efforts were focused on developing a sintering method which leads to better properties accompanying consuming less time in comparison with mentioned methods. Among sintering techniques, spark plasma sintering (SPS) is a reliable procedure to produce full dense ceramic bodies in a short time with high heating rates at low sintering temperature [7, 8]. SPS applies uniaxial pressure and DC pulsed current simultaneously in order to densify materials. Sample is located in a graphite die and DC pulsed current passes through the die and sample depending on material electrical conductivity [9, 10]. A wide range of optical ceramics has been produced successfully by SPS in recent decades, like Al_2O_3, $MgAl_2O_4$ spinel, Nd-YAG, Lu_2O_3 and MgO–Y_2O_3 nanocomposite [11–15].

Yoshida *et al.* [16] applied pressure of 83 MPa to densify Y_2O_3 disks by SPS with heating rate of 10°C/min. They observed an acceptable consolidation and a body with 97% relative density at 850°C. Yoshida *et al.* [17] have also spark plasma sintered Y_2O_3 under 80 MPa with heating rate of 2°C/min at 950°C and obtained a translucent body with 99% relative density. The bodies had 6–46% transmittance in 400–800 nm wavelength range.

Y_2O_3 ceramics mostly have been fabricated under uniaxial pressure of 100 MPa or more [18–23]. For this purpose, special grade of graphite should be utilised. These products are so expensive and are not simply accessible. Moreover, these high pressures influence on durability of graphite die because the strength of graphite is usually under 150 MPa [7] and makes it less durable and cause the final product cost increase. The SPS sintering temperature of Y_2O_3 mostly lies in the range 1000–1600°C [18–23]. In order to fabricate Y_2O_3 in low pressures, the temperature should be higher than what Yoshida *et al.* [17] reported to compensate low pressure. The effect of pressure on relative density is clear, but evaluation of pressure on other properties has seldom been discussed [22].

In the research reported in this Letter, we fabricated Y_2O_3 IR-transparent bodies via pressure lower than 100 MPa and investigated effect of pressure on densification, microstructure, IR transmission and mechanical properties.

2. Materials and methods: Y_2O_3 powder (purity 99.9%, Henan Huier Nano Technology Co., China) was used as the starting material. Particle size distribution was characterised by Zeta sizer (HS_A3000, Malvern, UK). Six gram of the powder was poured into a graphite die with 2 cm inner diameter which its inner and punch surfaces were covered by graphite foils before. A graphite felt blanket around the die was used to prevent heat losses. The powder was sintered by SPS machine (SPS-20 T-10, Easy Fashion metal products trade Co., China) in vacuum atmosphere with the residual pressure around 20 Pa. The temperature was measured by an optical pyrometer (Raytek, USA) adjusted on top of the lower punch surface. A pressure of 20 MPa was pre-loaded between room temperature and 1200°C and then it was increased to 80 or 90 MPa and held for 45 min at 1300°C. Average heating rate during SPS process was about 50°C/min. The samples were called sample80 and sample90. Density of the samples was measured by the Archimedes method in distilled water assuming theoretical density of 5.031 g/cm^3 [23]. Sintered sample90 was annealed at 1050°C for 6 h. Both sides of specimens were ground and polished up to 1 μm by diamond paste. In order to prepare microstructure figures, samples were thermally etched at 1225°C for 2 h. X-ray diffraction (XRD) examination was carried out by XRD (PW3710, Philips, Netherlands) using Cu Kα radiation (wavelength: 0.154 nm). IR transmission was evaluated before and after annealing by a Fourier-transform infrared (FTIR) spectrophotometer (Vector 33, Bruker Biospin Corp, USA) in the wavelength between 2.5 and 20 μm. Microstructure observations were done by a field emission scanning electron microscope (FESEM, TESCAN Mira 3-XMU, Czech Republic). The average grain size of Y_2O_3 samples was determined from linear intercept length of 100 grains in the FESEM images assuming that grain size is 1.56 times larger than the mean intercept [24]. Vickers hardness was measured by a UV1 Koopa hardness tester at a load of 1 kg with 10 s dwell time at room temperature. The average hardness value was attained from at least five indents for each sample. The fracture toughness was obtained from (1) where E is the elastic modulus of Yttria (170 GPa [25]), H_V is the Vickers hardness, P is the load during hardness test and C is the half length of crack made around the corners of the Vickers indentation [26]

$$K_{IC} = 0.016 \left(\frac{E}{H_V}\right)^{1/2} \frac{P}{C^{3/2}} \quad (1)$$

© The Institution of Engineering and Technology 2016

doi: 10.1049/mnl.2016.0218

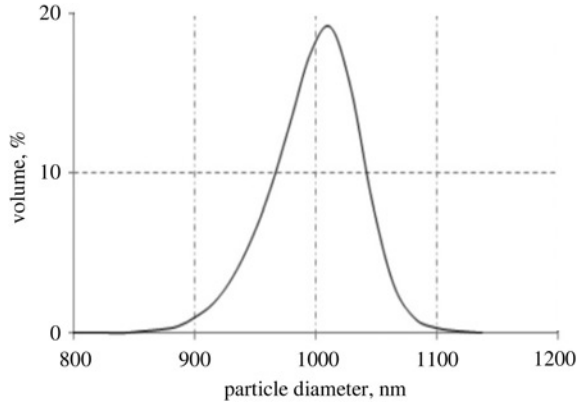

Fig. 1 *Particle size distribution of the as-received powder*

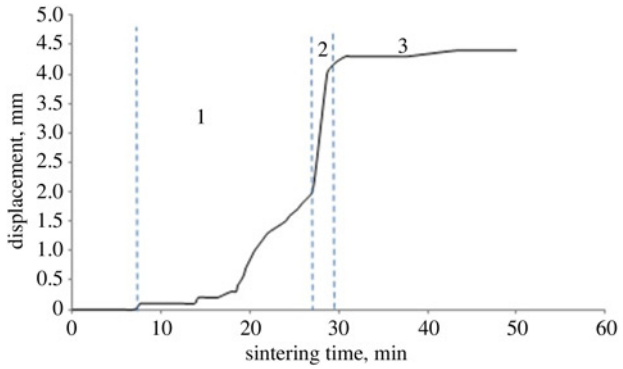

Fig. 3 *Displacement against time diagram of sample90. (1) first, (2) second, (3) third step of sintering*

3. Results and discussion

3.1. Sintering process: As-received powder had a narrow particle size distribution and its average particle size was 0.97 µm according to Fig. 1. Fig. 2 shows the XRD pattern of the Y_2O_3 powder. In this pattern, all reflections were attributed to the cubic Y_2O_3 (JCPDS Card No. 00-001-0831) with the space group number of 206 [27]. The relative densities of 97.03% ± 0.90% and 99.05% ± 0.90% were obtained for sample80 and sample90, respectively. It seems that, higher pressures led to the higher relative density. Pressure contributes for densification in two ways: first, mechanical function that progress sintering by rearranging powder particles and annihilation of agglomerates; second, intrinsic function which higher pressures can increase driving force for sintering process. It should be mentioned that effect of pressure on driving force of sintering is more tangible concerning coarser nanograined powder particles [28]. Hence, by increasing pressure, both mechanical and intrinsic functions can work better. It is worth to note that in sample80 the pressure was equal to what Yoshida *et al.* [17] applied, but the temperature and heating rate were 350°C and 48°C/min higher than their parameters, respectively. However, they had obtained bodies with 99% relative density but here sample80 has just 97.03% relative density which is in conflict with what Yoshida *et al.* [17] reported.

Fig. 3 shows the diagram of displacement against time of sample90. Prior to initiate sintering, the pressure of 20 MPa was applied in order to prohibit contamination of graphite with powder. After about 10 min, in the first step of sintering the powder particles moved and rearranged to be packed together and a slight shrinkage was noticed [19]. After 20 min, when the temperature was about 1000°C, a significant slope was observed up to 1300°C. Once the temperature reached to 1200°C, the pressure gradually increased up to 90 MPa until temperature became 1300°C. As the sintering temperature evaluated by pyrometer was below 1400°C, the reason of intensive densification may not attribute to plastic deformation [18]. On the other hand, at temperature above 600°C, radiation of inner wall of die is significant and the exact temperature of sample may be higher than 1300°C or even 1400°C [16]. Thus, plastic deformation may be the reason of fast densification here. Other mechanisms like nanograin-coalescense sliding may bring out fast densification too [7]. In the second step of sintering, when pressure was applied and the die surface temperature reached 1300°C, it seems that a viscous layer was created around particle surfaces, which contributes to grain sliding or nanograin-coalescense sliding, and drastic displacement was observed [7, 19]. Seemingly in the third step, when the temperature was constantly 1300°C, sintering continued by diffusion and grain growth mechanism but displacement slightly increased because of time-consuming grain boundary diffusion process [19].

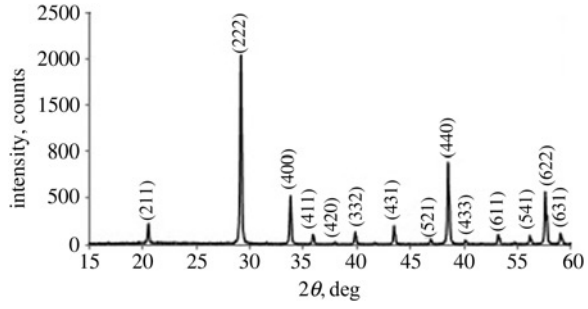

Fig. 2 *XRD pattern of the as-received powder*

3.2. Microstructure: Fig. 4 shows the microstructure of sample80 (after sintering) and sample90 (after annealing). It can be seen that in sample90, in spite of annealing, by increasing pressure a finer microstructure was attained which may be due to applying pressure preclude from diffusion and grain growth during both sintering and annealing. According to Fig. 1, the average particle size of the starting powder was 0.97 µm and it is known that these powder particles consist of some grains, which grew during sintering (Fig. 4). By increasing pressure, relative density became greater and average grain size reduced (Table 1). During sintering, diffusion mechanism includes grain boundary and surface diffusion that the former one enhances by the number of pores and grain boundary diffusion proceeds by Y^{3+} diffusion. Therefore, less porosities result in slower surface diffusion and consequently lower grain growth and lower grain size [18]. In sample80, crack-like porosities (shown by arrows in Fig. 4*a*) were observed which can be the reason of low density of 97.03%.

3.3. Optical properties: Fig. 5 shows sample90 before and after annealing at 1050°C for 6 h. As-sintered sample has a darker part in the middle which may arise from the heterogeneity due to sintering by SPS. Since Y_2O_3 is a dielectric material, DC pulsed current only passed through the graphite die and punches. Therefore, edge of sample had higher temperature in comparison with its centre [10]. This case was also discussed by Xiong *et al.* [29] in the literature for spark plasma sintered AlN ceramic. The dark appearance originated from imperfections mostly oxygen ion vacancies and carbon diffusion from graphite foils [12]. The Y_2O_3 oxide ceramic has intrinsic oxygen defects itself because of its original crystallographic structure [30]. On the other hand, during SPS special conditions like vacuum and pulsed electric current were present to create more oxygen vacancies [22]. It seems that these vacant places interact with free electrons, and then colour centres (F, F^+) as described by (2) and (3) will be created. These colour centres have significant high absorption coefficient which absorb light drastically [31]. Therefore,

© The Institution of Engineering and Technology 2016

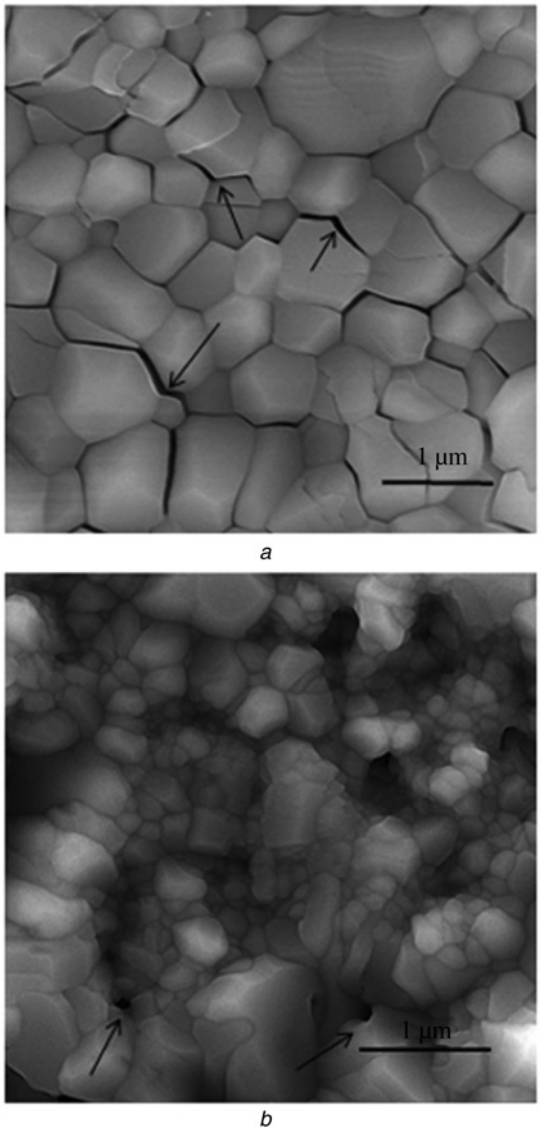

Fig. 4 *Microstructure of*
a As-sintered sample80
b Annealed sample90

as-sintered body was seen in dark grey colour

$$V_O^{\bullet\bullet} + e' \rightarrow V_O^{\bullet}(F^+) \quad (2)$$

$$V_O^{\bullet\bullet} + 2e' \rightarrow V_O^{\times}(F) \quad (3)$$

Sample80 did not transmit IR wavelength because of low relative density of 97.03%. By applying higher pressure and attaining higher relative density, the Y_2O_3 body transmitted IR waves. Fig. 6 shows the FTIR transmission of sample90 before and after annealing at 1050°C for 6 h. As-sintered sample90 had a transmission of 20–34% in the wave number range of 3333–2000 cm^{-1} (3–5 μm). This low transmission of the IR waves originated from absorption of light by oxygen vacancies and remained porosities (shown by arrows in Fig. 4*b*). In order to eliminate these defects, annealing in air was suggested. An *et al.* [23] also reported the positive influence of annealing process. They obtained 1050°C temperature which led to the best result. Hence, annealing temperature of 1050°C was chosen here. After annealing at 1050°C for 6 h, the transmission proceeded and become in the range of 50–60% in the wave number range of 3333–2000 cm^{-1} (3–5 μm). After annealing, absorption peaks of 1502 and 1416 cm^{-1} appeared may be due to absorption of carbonate groups from air or formation and entrapment of CO or CO_2 gases in the sample according to graphite penetration [12, 14]. These peaks around 6.6 μm were also observed for annealed Lu_2O_3 and MgO–Y_2O_3 nanocomposite [14, 15].

Table 1 Hardness and fracture toughness of sample80 and sample90

Sample	Sample80	Sample90 annealed at 1050°C
relative density, %	97.03 ± 0.90	99.05 ± 0.90
hardness, GPa	9.19 ± 0.16	9.37 ± 0.26
fracture toughness, MPa.$m^{1/2}$	1.47 ± 0.01	1.60 ± 0.05
average grain size, μm	0.97 ± 0.08	0.76 ± 0.12

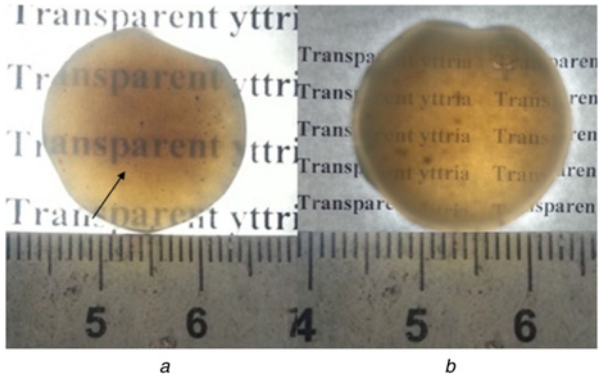

Fig. 5 *Appearance of sample90*
a Before annealing at 1050°C for 6 h
b After annealing at 1050°C for 6 h
Text is 30 mm under sample in *b*

3.4. Mechanical properties: To investigate the mechanical properties of the sintered samples, their hardness and fracture toughness were evaluated (Table 1). Grain boundaries in the polycrystalline ceramics with fine microstructure are closed together; therefore the acquired space does not exist for mobility of defects. Hence, hardness depends on grain size [32] and therefore smaller grains leads to the more hardness [33]. Although the grain size of sample90 was lower than sample80, and sample90 had higher relative density, these samples had approximately same hardness and their difference can be neglected. Hardness of 8.8 ± 0.2 GPa for Y_2O_3 dense body with the average grain size of 0.76 μm was reported by Albayrak *et al.* [34] at 1 kg hardness testing load which is in consistence with our results.

The values of fracture toughness showed that it is sensitive to grain size. Grain size influences the fracture toughness more than

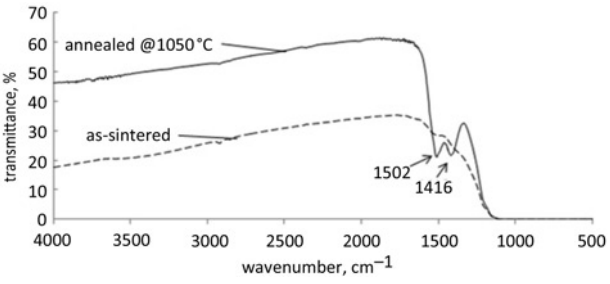

Fig. 6 *FTIR transmission of sample90 before and after annealing at 1050°C for 6 h. The thickness of sample is about 3.5 mm*

© The Institution of Engineering and Technology 2016

doi: 10.1049/mnl.2016.0218

hardness. Smaller grains have more grain boundaries which inhibit crack growth in the ceramic body [25] and consequently the fracture toughness increases. Fracture toughness of 1.3 ± 0.1 MPa.m$^{1/2}$ was calculated by Albayrak *et al.* [34] for the mentioned sample using (1) which is slightly lower than 1.60 ± 0.05 MPa.m$^{1/2}$ reported here for sample90. This difference may be due to their different preparation method for better observing of cracks, because polishing the surfaces with a 1 mm diamond paste after hardness test may cause crack growth.

4. Conclusion: IR-transparent Y_2O_3 was successfully produced by SPS. The sample sintered at 1300°C under 90 MPa with the heating rate of 50°C/min had transmission of 50–60% in the wavelength of 3–5 μm. Average grain size, hardness and fracture toughness of 0.76 μm, 9.37 GPa and 1.60 MPa.m$^{1/2}$ were attained for this sample, respectively. It was found that higher applied pressure resulted in finer microstructure and more desirable mechanical properties. Oxygen vacancies created in the as-sintered sample, and these imperfections could be lessened by annealing at 1050°C for 6 h.

5 References

[1] Lu Q., Yang Q., Lu S., *ET AL.*: 'Fabrication, structure refinement and EXAFS analysis of yttrium lanthanum oxide transparent ceramics', *Opt. Mater.*, 2014, **36**, pp. 1289–1294

[2] Gan L., Park Y.J., Park M.J., *ET AL.*: 'Facile fabrication of highly transparent yttria ceramics with fine microstructures by a hot-pressing method', *J. Am. Ceram. Soc.*, 2015, **98**, pp. 2002–2004

[3] Futami Y., Yanagida T., Fujimoto Y., *ET AL.*: 'Optical and scintillation properties of Sc_2O_3, Y_2O_3 and Lu_2O_3 transparent ceramics synthesized by SPS method', *Radiat. Meas.*, 2013, **55**, pp. 136–140

[4] Gupta Y.M., Eilers H., Chaudhuri S., *ET AL.*: 'Characterization and development of advanced materials: role & understanding of interfacial phenomena (congressional), DTIC document'. Report No. N00014-03-1-0247, December 2007

[5] Zhang L., Feng J., Pan W.: 'Vacuum sintering of transparent Cr: Y_2O_3 ceramics', *Ceram. Int.*, 2015, **41**, pp. 8755–8760

[6] Mouzon J., Maitre A., Frisk L., *ET AL.*: 'Fabrication of transparent yttria by HIP and the glass-encapsulation method', *J. Eur. Ceram. Soc.*, 2009, **29**, pp. 311–316

[7] Chaim R.: 'Densification mechanisms in spark plasma sintering of nanocrystalline ceramics', *Mater. Sci. Eng. A*, 2007, **443**, pp. 25–32

[8] Chaim R., Levin M., Shlayer A., *ET AL.*: 'Sintering and densification of nanocrystalline ceramic oxide powders: a review', *Adv. Appl. Ceram.*, 2008, **107**, pp. 159–169

[9] Diouf S., Molinari A.: 'Densification mechanisms in spark plasma sintering: effect of particle size and pressure', *Powder Technol.*, 2012, **221**, pp. 220–227

[10] Vanmeensel K., Laptev A., Hennicke J., *ET AL.*: 'Modelling of the temperature distribution during field assisted sintering', *Acta Mater.*, 2005, **53**, pp. 4379–4388

[11] Kim B.N., Hiraga K., Morita K., *ET AL.*: 'Spark plasma sintering of transparent alumina', *Scr. Mater.*, 2007, **57**, pp. 607–610

[12] Morita K., Kim B.N., Yoshida H., *ET AL.*: 'Spectroscopic study of the discoloration of transparent $MgAl_2O_4$ spinel fabricated by spark-plasma-sintering (SPS) processing', *Acta Mater.*, 2015, **84**, pp. 9–19

[13] Frage N., Kalabukhov S., Sverdlov N., *ET AL.*: 'Effect of the spark plasma sintering (SPS) parameters and LiF doping on the mechanical properties and the transparency of polycrystalline Nd-YAG', *Ceram. Int.*, 2012, **38**, pp. 5513–5519

[14] An L., Ito A., Goto T.: 'Effects of ball milling and post-annealing on the transparency of spark plasma sintered Lu_2O_3', *Ceram. Int.*, 2011, **37**, pp. 2263–2267

[15] Jiang D., Mukherjee A.K.: 'The influence of oxygen vacancy on the optical transmission of an yttria–magnesia nanocomposite', *Scr. Mater.*, 2011, **64**, pp. 1095–1097

[16] Yoshida H., Morita K., Kim B.N., *ET AL.*: 'Densification of nanocrystalline yttria by low temperature spark plasma sintering', *J. Am. Ceram. Soc.*, 2008, **91**, pp. 1707–1710

[17] Yoshida H., Morita K., Kim B.N., *ET AL.*: 'Low-temperature spark plasma sintering of Yttria ceramics with ultrafine grain size', *J. Am. Ceram. Soc.*, 2011, **94**, pp. 3301–3307

[18] Chaim R., Shlayer A., Estournes C.: 'Densification of nanocrystalline Y_2O_3 ceramic powder by spark plasma sintering', *J. Eur. Ceram. Soc.*, 2009, **29**, pp. 91–98

[19] Marder R., Chaim R., Estournès C.: 'Grain growth stagnation in fully dense nanocrystalline Y_2O_3 by spark plasma sintering', *Mater. Sci. Eng. A*, 2010, **527**, pp. 1577–1585

[20] Marder R., Chaim R., Chevallier G., *ET AL.*: 'Effect of 1wt% LiF additive on the densification of nanocrystalline Y_2O_3 ceramics by spark plasma sintering', *J. Eur. Ceram. Soc.*, 2011, **31**, pp. 1057–1066

[21] Marder R., Chaim R., Chevallier G., *ET AL.*: 'Densification and polymorphic transition of multiphase Y_2O_3 nanoparticles during spark plasma sintering', *Mater. Sci. Eng. A*, 2011, **528**, pp. 7200–7206

[22] Zhang H., Kim B.N., Morita K., *ET AL.*: 'Fabrication of Transparent Yttria by high-pressure spark plasma sintering', *J. Am. Ceram. Soc.*, 2011, **94**, pp. 3206–3210

[23] An L., Ito A., Goto T.: 'Transparent yttria produced by spark plasma sintering at moderate temperature and pressure profiles', *J. Eur. Ceram. Soc.*, 2012, **32**, pp. 1035–1040

[24] Mendelson M.I.: 'Average grain size in polycrystalline ceramics', *J. Am. Ceram. Soc.*, 1969, **52**, pp. 443–446

[25] Kaminskii A., Akchurin M.S., Gainutdinov R., *ET AL.*: 'Microhardness and fracture toughness of Y_2O_3-and $Y_3Al_5O_{12}$-based nanocrystalline laser ceramics', *Crystallogr. Rep.*, 2005, **50**, pp. 869–873

[26] Green D.J.: 'An introduction to the mechanical properties of ceramics' (Cambridge University Press, Cambridge, UK, 1998), pp. 243–244

[27] Hanawalt J.D., Rinn H.W., Frevel L.K.: 'Chemical analysis by X-ray diffraction', *Anal. Chem.*, 1938, **10**, p. 475

[28] Munir Z., Anselmi-Tamburini U., Ohyanagi M.: 'The effect of electric field and pressure on the synthesis and consolidation of materials: a review of the spark plasma sintering method', *J. Mater. Sci.*, 2006, **41**, pp. 763–777

[29] Xiong Y., Fu Z., Wang H., *ET AL.*: 'Microstructure and IR transmittance of spark plasma sintering translucent AlN ceramics with CaF_2 additive', *Mater. Sci. Eng. B*, 2005, **123**, pp. 57–62

[30] Chen P.L., Chen I.W.: 'Grain boundary mobility in Y_2O_3: defect mechanism and dopant effects', *J. Am. Ceram. Soc.*, 1996, **79**, pp. 1801–1809

[31] Zhang W., Lu T., Wei N., *ET AL.*: 'Effect of annealing on the optical properties of Nd: YAG transparent ceramics', *Opt. Mater.*, 2012, **34**, pp. 685–690

[32] Pelleg J.: 'Mechanical properties of ceramics' in Gladwell G.M.L. (ed.): 'Mechanical properties of ceramics' (Springer Science & Business, New York, 2014), vol. 213, pp. 127–129

[33] Krell A.: 'A new look at the influences of load, grain size and grain boundaries on the room temperature hardness of ceramics', *Int. J. Refract. Met. Hard Mater.*, 1998, **16**, pp. 331–335

[34] Albayrak I.C., Basu S., Sakulich A., *ET AL.*: 'Elastic and mechanical properties of polycrystalline transparent yttria as determined by indentation techniques', *J. Am. Ceram. Soc.*, 2010, **93**, pp. 2028–2034

© The Institution of Engineering and Technology 2016